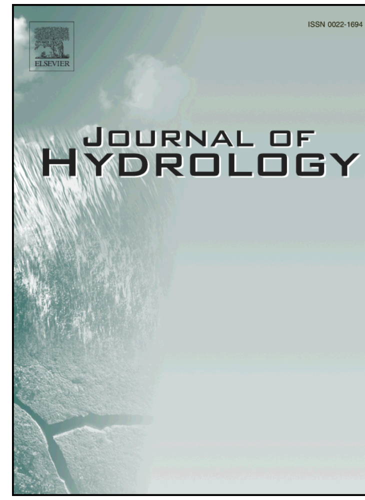

Research papers

The added value of stochastic spatial disaggregation for short-term rainfall forecasts currently available in Canada

Patrick Gagnon, Alain N. Rousseau, Dominique Charron, Vincent Fortin, René Audet

PII: S0022-1694(17)30549-8
DOI: http://dx.doi.org/10.1016/j.jhydrol.2017.08.023
Reference: HYDROL 22186

To appear in: *Journal of Hydrology*

Received Date: 4 January 2017
Revised Date: 10 August 2017
Accepted Date: 14 August 2017

The added value of stochastic spatial disaggregation for short-term rainfall forecasts currently available in Canada

Patrick Gagnon[a1], Alain N. Rousseau[b*], Dominique Charron[c], Vincent Fortin[d], René Audet[e]

[a]Agriculture and Agri-Food Canada, 2560 Hochelaga blvd, Québec city, Qc, Canada, G1V 2J3. patrick.gagnon@agr.gc.ca

[b]Institut National de la Recherche Scientifique, Centre Eau Terre Environnement, 490 rue de la Couronne, Québec city, Qc, Canada, G1K 9A9. alain.rousseau@ete.inrs.ca ([*]Corresponding author)

[c]Institut National de la Recherche Scientifique, Centre Eau Terre Environnement, 490 rue de la Couronne, Québec city, Qc, Canada, G1K 9A9. dominique.charron@ete.inrs.ca

[d]Environment and Climate Change Canada, 2121 route Transcanadienne, Dorval, Qc, Canada, H9P 1J3. vincent.fortin@canada.ca

[e]Agriculture and Agri-Food Canada, 2560 Hochelaga blvd, Québec city, Qc, Canada, G1V 2J3. rene.audet@agr.gc.ca

[1] Current address: Centre de développement du porc du Québec inc. Place de la Cité, Belle Cour tower, 2590 Laurier blvd, office 450, Québec city, Québec, G1V 4M6, pgagnon@cdpq.ca

Abstract

Several businesses and industries rely on rainfall forecasts to support their day-to-day operations. To deal with the uncertainty associated with rainfall forecast, some meteorological organisations have developed products, such as ensemble forecasts. However, due to the intensive computational requirements of ensemble forecasts, the spatial resolution remains coarse. For example, Environment and Climate Change Canada's (ECCC) Global Ensemble Prediction System (GEPS) data is freely available on a 1-degree grid (about 100 km), while those of the so-called High Resolution Deterministic Prediction System (HRDPS) are available on a 2.5-km grid (about 40 times finer). Potential users are then left with the option of using either a high-resolution rainfall forecast without uncertainty estimation and/or an ensemble with a spectrum of plausible rainfall values, but at a coarser spatial scale. The objective of this study was to evaluate the added value of coupling the Gibbs Sampling Disaggregation Model (GSDM) with ECCC products to provide accurate, precise and consistent rainfall estimates at a fine spatial resolution (10-km) within a forecast framework (6-hours). For 30, 6-h, rainfall events occurring within a 40,000-km^2 area (Québec, Canada), results show that, using 100-km aggregated reference rainfall depths as input, statistics of the rainfall fields generated by GSDM were close to those of the 10-km reference field. However, in forecast mode, GSDM outcomes inherit of the ECCC forecast biases, resulting in a poor performance when GEPS data were used as input, mainly due to the inherent rainfall depth distribution of the latter product. Better performance was achieved when the Regional Deterministic Prediction System (RDPS), available on a 10-km grid and aggregated at 100-km, was used as input to GSDM. Nevertheless, most of the analyzed

ensemble forecasts were weakly consistent. Some areas of improvement are identified herein.

Highlights

- GSDM applied on reference data generates accurate and precise rainfall fields
- GSDM inherits the forecast bias
- Global ensemble forecasts (GEPS) are not consistent, with or without GSDM
- GSDM performance was better with regional deterministic forecasts (RDPS)
- Neighboring pixels should be considered when producing high-resolution ensembles

Keywords

Gibbs Sampling Disaggregation Model (GSDM), Canadian Precipitation Analysis (CaPA), Global Ensemble Prediction System (GEPS), Regional Deterministic Prediction System (RDPS), ensemble, high-resolution rainfall.

1 Introduction

Numerous businesses and industries need consistent, precise and accurate, high-resolution, short-term rainfall forecasts. For example, in urban areas, high-resolution rainfall forecasts are of interest for stormwater management (*e.g.*, Gaborit *et al.*, 2014). They are also important in rural areas where agricultural activities (e.g., fungicide applications, some herbicides applications, hay harvesting, manure application, irrigation management), that are affected by local rainfall depth, require up-to-the-hour information (*e.g.*, Cai *et al.*, 2007; Silva *et al.*, 2010; Cai *et al.*, 2011; Bendre *et al.*, 2015).

Thanks to advances in computational resources, understanding and parameterization of key physical processes, increased access to satellite data, and data assimilation techniques, meteorological models have made tremendous strides in the last decades (Bauer *et al.*, 2015). One of the most spectacular changes that has occurred is an impressive increase in horizontal resolution. For example, the horizontal resolution of Environment and Climate Change Canada's (ECCC) global deterministic prediction system has improved from approximately 150-km in 1990 to 25-km in 2013 (changes to ECCC's operational model are documented at: http://collaboration.cmc.ec.gc.ca/cmc/cmoi/product_guide/docs/changes_e.html). Throughout Canada, deterministic forecasts are routinely issued on a grid having a horizontal resolution of 2.5 km. The accuracy of the forecasts has improved accordingly. For example, based on the root mean-squared-error (RMSE) of the 850 hPa temperature forecasts issued by ECCC over North America, a 3-day forecast issued in 2015 was about as accurate as a 1-day forecast issued in 1995, and a 5-day forecast issued in 2015 was about as accurate as a 3-day forecast issued in 1995. This corresponds to a gain of approximately one day of lead time per decade, which is consistent with improvements reported by Bauer et al. (2015) for the European Centre for Medium-Range Weather Forecasts.

Despite significant advances (e.g., COSMO forecast system; Baldauf *et al.*, 2011), it remains difficult to get reliable rainfall forecasts for fine spatiotemporal scales. To circumvent this issue, meteorological organisations are developing ensemble products that provide several forecasts for a given timeframe; providing a spectrum of rainfall depths associated with model uncertainty. However, because of the ensuing computational requirements, the spatial resolution is generally coarser than that of a deterministic run. Furthermore, outputs are not always made available on the original model grid due to disk space constraints. For example, the Canadian ensemble forecasts from the Global Ensemble Prediction System (GEPS) of ECCC, which are issued on a 50-km grid, are freely available on a 1-degree grid (about 100 km), while the spatial resolution of their High Resolution Deterministic Prediction System (HRDPS) is about 40 times finer (2.5 km at 60°N). Thus, there is still a wide gap between available forecasts and stakeholder requirements, namely: (i) rainfall estimates close to actual, local-scale values, (ii) information about the uncertainty of local estimates, and for some applications, (iii) available data for short-term decisions.

Meanwhile, rainfall and weather generators can both produce fine-scale rainfall fields from coarse meteorological and/or climate simulations (*e.g.*, Paschalis *et al.*, 2013; Peleg and Morin, 2014; Niemi *et al.*, 2016). However, the goal of most applications is to generate scenarios for long-term predictions. Alternatively, disaggregation models which can generate rapidly several fine-scale rainfall fields from one coarse scale field represent a promising avenue for short-term forecasts.

During the past decades, several studies have focused on spatial distribution of rainfall at fine scale (Gupta and Waymire, 1993; Hubert *et al.*, 1993; Kumar and Foufoula-Georgiou, 1993a,b; Marsan *et al.*, 1996; Olson and Niemczynowicz, 1996; among others). An approach commonly used by disaggregation models is to divide in cascade each grid cell in 2x2 pixels, which are then divided in 2x2 sub-pixels, so on so forth (*e.g.*, Over and Gupta, 1996; Perica and Foufoula-Georgiou, 1996; Deidda, 2000; Harris and Foufoula-Georgiou, 2001; Badas *et al.*, 2006; Deidda *et al.*, 2006a,b; Gaborit *et al.*, 2014; among others). These models are conceptually simple, but may lead to unrealistic rainfall fields with visible discontinuities, due to the discretization of the space (Lovejoy and Schertzer, 2010a,b). Gagnon *et al.* (2012) proposed a stochastic disaggregation model, hereafter referred to as the Gibbs Sampling Disaggregation Model (GSDM), which does not produce discontinuities, even for adjacent pixels from two different grid cells (Figure 1). The model was adapted for orographic rainfall (Gagnon *et al.*, 2013) and used to evaluate the impact of climate change on extreme rainfall events over a small watershed (Gagnon and Rousseau, 2014). Nevertheless, the model has never been applied for short-term meteorological forecasts.

The general objective of this study was to evaluate the capability of GSDM coupled with ECCC products to provide accurate, precise and consistent rainfall estimates within a short time frame. The specific objectives were to:

(i) Evaluate accuracy, precision and consistency of GSDM when applied on aggregated reference rainfall fields;

(ii) Compare two freely-available ECCC rainfall forecasts, a deterministic and an ensemble forecast, to a reference rainfall product (namely CaPA, *cf* Section 2.2);

(iii) Determine the added value of coupling GSDM to these ECCC forecasts;

(iv) Identify possible modifications to GSDM potentially leading to improved forecasts.

This study focused on 30, 6-h, rainfall events that occurred between July and November 2015 over a 40,000-km^2 area on the south shore of the St. Lawrence River, Québec, Canada.

2 Materials and Methods

2.1 Study Area

The region of interest consists of an area approximately 200 x 200 km^2, from 45 to 47° N and from 71 to 73° W, covering the watershed of the Bécancour River on the south shore of the St. Lawrence River in Québec, Canada (Figure 2). Primarily located in the St. Lawrence Lowlands, only the upstream southeastern portion is in the Appalachian Mountains. The climate is continental humid (Dfb under Köppen classification) with the highest precipitation during the months of July, August and September. Around 40% of the area, mainly in the Lowland sector, is occupied by agricultural activities that would benefit from better local-scale rainfall forecasts. With respect to GDSM data requirements, the modeled area spans from 44 to 48° N and from 70 to 74° W (study area ± 1° in each direction). In this manuscript, a grid cell refers to the spatial unit of a grid with 1° (about 100-km) resolution and pixel refers to a spatial unit of a 10-km grid (see Figure 2).

2.2 Environment and Climate Change Canada products

Three different ECCC products, all freely available on the web (https://weather.gc.ca/grib/index_e.html), were used. First, the Canadian Precipitation Analysis (CaPA; Fortin *et al.*, 2015) was identified as the reference (pseudo-observed) precipitation. CaPA uses short-term forecasts as a background field and assimilates data from various sources (stations, radars, satellites). The background field is modified by spatial interpolation (kriging) of the difference between the forecast and the observations. The dataset has a spatial resolution of 10 km x 10 km on a polar stereographic grid covering North America. For this study, the computational domain consisted of a 40x40-pixel grid (Figure 2) overlaying the area of interest (44-48°N and 70-74°W), oriented east-west, by taking the closest pixel from the original grid.

Second, the Regional Deterministic Prediction System (RDPS; Caron *et al.*, 2015) forecasts on the same grid as that of CaPA, similarly transposed on the 40x40-pixel grid oriented east-west. It is important to note that RDPS provides the background field to CaPA, the reference precipitation, and thus it could be an advantage for RDPS compared to another product. That being said, the dense observation network and the radar in the region analyzed provided sufficient data limiting the contribution of RDPS in CaPA. It is thus assumed that the advantage of RDPS, if any, is negligible for the studied region.

The third and final product was the Global Ensemble Prediction System (GEPS; Charron *et al.*, 2010; Houtemaker *et al.*, 2014) which produces 21 forecasts on a 1° x 1° (about 100 km x 100 km) grid. The 21 members are formed by one control member and 20 perturbed members, having different physical parameterization, data assimilation cycles and initial observed conditions.

In addition to rainfall depth, three input atmospheric variables required by GSDM (Section 2.3) were obtained from RDPS and GEPS forecasts: (i) convective available potential energy (CAPE), (ii) wind speed and (iii) wind direction at the 700-hPa pressure level.

CaPA and GEPS data are available at a 6-h time step, while RDPS data at a 3-h time step, but aggregated at 6-h time step (sum for rainfall depth, average for wind speed and CAPE). For GEPS, since simulations are launched twice a day, the required data covered two forecast periods: (i) the first 6 hours and (ii) from 6 to 12 hours following the start of the simulations. The same strategy is used for the RDPS, although RDPS forecasts are available four times per day.

Two individual periods were analyzed for GSDM calibration and evaluation of rainfall products. The calibration period covered May through October 2014 as well as May and June 2015. Each CaPA grid point that received at least 1 mm of rain during a 6-h time step was retained for calibration, for a total of 208,766 pixels. Atmospheric variables (CAPE and wind at 700 hPa) were retrieved from RDPS forecasts. Evaluation of ECCC products (Section 2.4) spanned from July to November 2015. A total of 30, 6-h time steps with the largest mean GEPS forecasted accumulations were retained (Table 1).

Note that ECCC has other forecast products that could be of interest, but were not included in the present study such as the High Resolution Deterministic Prediction System (HRDPS; Mailhot *et al.*, 2010), having a 2.5-km resolution. Also, the Regional

Ensemble Prediction System (REPS; Charron *et al.*, 2013) having grid spacing of 15-km and a lead time of 72-h, with two integrations per day and 21 ensemble members, was not included since the data is not freely available. Moreover, it could be difficult to retrieve in a timely fashion for actual short-term forecasts.

2.3 Gibbs Sampling Disaggregation Model (GSDM)

The model assumed that $R_{i,j}$, the rainfall depth at a given 10-km pixel (i,j) for a given 6-h period, is a random variable with expected value μ and standard deviation σ given by (Gagnon, 2012; Gagnon and Rousseau, 2014):

$$\mu = \overline{A} + \beta_d \left(\frac{A_{-} + A_{|}}{2} - \frac{A_{/} + A_{\backslash}}{2} \right) + \beta_v V \left[\cos\left(2\left(W - 45^{\circ}\right)\right)\left(A_{/} - A_{\backslash}\right) + \cos\left(2\left(W - 90^{\circ}\right)\right)\left(A_{|} - A_{-}\right) \right]$$

(1)

$$\sigma = \left(\beta_0 + \beta_1 C\right)\mu^{\beta_2} \qquad (2)$$

where $\overline{A}$ is the mean rainfall depth of the eight surrounding pixels and the other A's are mean rainfall depths in the four directions, namely $A_{/} = \dfrac{R_{i-1,j-1} + R_{i+1,j+1}}{2}$, $A_{|} = \dfrac{R_{i-1,j} + R_{i+1,j}}{2}$, $A_{\backslash} = \dfrac{R_{i-1,j+1} + R_{i+1,j-1}}{2}$, and $A_{-} = \dfrac{R_{i,j-1} + R_{i,j+1}}{2}$, V is the 700-hPa wind speed (m/s), W is the 700-hPa wind direction (degree), C stands for CAPE (J/kg), and the five calibration parameters are: β_d (dimensionless), β_v (s/m), β_0 (mm), β_1 (mm kg/J), and β_2 (dimensionless). As in many rainfall models (*e.g.*, Over and Gupta, 1996; Fiorucci *et al.*, 2001; Forman *et al.*, 2008; Groppelli *et al.*, 2011), a lognormal distribution is assumed for $R_{i,j}$. In these equations, it is assumed that strong 700-hPa winds might lead to anisotropy and high CAPE values increase spatial variability (*i.e.*, decrease the influence of the neighboring pixels).

The model can disaggregate at any spatial resolution, but it is recommended to target a resolution at which rainfall depths are available for calibration. In this study, 10-km 6-h rainfall depths from 208,766 pixels from CaPA analyses were used for calibration (Section 2.2). The estimated values for parameters β_d and β_v of Equation (1) minimizes the sum of the squared differences between observed rainfall depths and expected rainfall depths calculated using Equation (1) for all pixels used for calibration (Gagnon, 2012; Gagnon *et al.*, 2012). Then, groups were created from all calibration pixels; all pixels within a group had similar expected rainfall depths and CAPE values. For each group, mean expected rainfall depth and mean CAPE value were calculated. The estimated values for parameters β_0, β_1, and β_2 of Equation (2) minimizes the sum of the squared differences between the observed 99.9% quantile of rainfall depths in each group and the 99.9% quantile calculated using the lognormal distribution with mean expected rainfall depth for each group and standard deviation given by Equation (2) (with mean CAPE value for each group and calibration parameters). Fitting the 99.9% quantile was done to attenuate the underdispersion of the lognormal distribution for rainfall depth estimation (Gagnon *et al.*, 2012; Gagnon and Rousseau, 2014).

Equations (1) and (2) allow rainfall depths to be generated on a 10-km pixel when neighboring depths are known. However, in practice, only coarse scale (100 km in this study) data is available as input to the disaggregation model. An algorithm based on the Gibbs sampling theory (Geman and Geman, 1984; Roberts and Smith, 1994) was developed to circumvent this issue. First, as initial conditions, the rainfall depth for each

10-km pixel was set to the rainfall depth of the 100-km grid cell covering the pixel. Then, new rainfall depths were generated from the lognormal distribution using Equations (1) and (2) for each 10-km pixel, one at the time. An *iteration* is completed when all pixels have been updated once. After each iteration, a multiplicative factor (generally close to 1) was applied to ensure that the model preserved the exact rainfall depth of each 100-km grid cell used as input. Based on the Gibbs sampling theory (Geman and Geman, 1984; Roberts and Smith, 1994), the rainfall depth on each 10-km pixel is approximately distributed using the lognormal distribution along with Equations (1) and (2) after a sufficient number of iterations. In this study, 300 iterations were performed before retaining the first disaggregated rainfall field, referred to as the first *realization*. Since fields from consecutive iterations are autocorrelated, subsequent realizations were separated by 100 iterations. The model is not explicitly made to generate spatial rainfall intermittency (*i.e.*, pixels without rain), but this can be achieved by setting to 0 those rainfall depths below a given threshold (0.1 mm in the present work). A detailed description of the algorithm is provided in Gagnon (2012), Gagnon *et al*. (2012) and Gagnon and Rousseau (2014).

2.4 Products analyzed

For each one of the 30, 6-h, rainfall events retained (Section 2.2), a total of 13 different rainfall products were analyzed (Table 2). These products were referenced with respect to the ECCC product used ("C" for CaPA analyses, "R" for RDPS forecasts and "G" for GEPS forecasts), whether aggregation and/or disaggregation was performed ("d" for 10-km disaggregated product, "a" for 100-km aggregated product without disaggregation), and whether neighboring pixels were used to create an ensemble ("n" if so).

The original 10-km CaPA rainfall (C) became the reference (true value) for the 12 other series. GSDM was first applied with aggregated CaPA data (Ca) as input. The ensuing product (Cd) compared to the reference (C) evaluates the performance of the disaggregation model. Comparison of the outcomes of Cd with Ca was used to assess the added value of GSDM over a low-resolution product.

One of the strength of GSDM is that it can generate realistic spatial patterns, even with 100-km grid cells used as input. However, it cannot always be right at the exact location (10-km pixel) since no fine scale information is used as input. Thus, it was decided to evaluate another disaggregated ensemble product, which instead of considering only the rainfall depths generated at the target pixel (as for Cd), it also includes the rainfall depths in the neighboring area (Cdn; 100 model realisations x 121 pixels [+/- 5 pixels in each direction] = 12,100 rainfall depths per 10-km pixel per 6-h event). The ensembles Cd and Cdn were also compared with the ensemble formed by the CaPA rainfall depths in 120 neighboring pixels (+/- 5 pixels in each direction - the target pixel; Cn, Table 2). This latter ensemble was used to evaluate whether neighboring pixels could actually be used for suitable estimation of the rainfall depth of the target pixel in this area.

Eight forecast products were compared. For both RDPS and GEPS forecasts, analyses were performed on rainfall depths from raw products (referred to as R and G, respectively), in order to evaluate the actual forecasts available for an end user. Then, disaggregation at the target pixel (Rd and Gd) and disaggregation in the neighboring area (Rdn and Gdn) was performed to evaluate the added value of GSDM coupled with the forecasts. For RDPS, it required data aggregation (Ra) prior disaggregation. For a given pixel, RDPS outcomes in the neighboring area (+/- 5 pixels in each direction; Rn) were also analyzed. The interest in Rn lies in the construction of an ensemble from a deterministic forecast requiring no additional computational time, contrary to disaggregation.

2.5 Performance evaluation

The performance of a product was assumed to vary depending on the reference rainfall depth (large rainfall depths being more difficult to correctly place spatially) and on the type of events (stratiform or convective events being governed by different physical processes). Seven groups, based on these two variables, were constructed (Table 3) and performance metrics calculated independently for each group.

Three criteria were accounted for in the evaluation: accuracy, precision and, for stochastic products only, consistency. Accuracy refers to bias, that is the mean difference between simulated and observed values. Precision is defined in two ways. Precision of a probabilistic product is related to the variability (range) of the realizations. Precision of the error, for a deterministic or probabilistic product, is related to the variability of the difference between the prediction and the reference. Finally, consistency is when the reference value is indistinguishable from a randomly selected member of an ensemble (Anderson, 1997).

For all products, deterministic or probabilistic, the Mean Squared Error (MSE) was calculated. For a given group with n pixels (Table 3) and a given rainfall product, let x_1, …, x_n be the reference rainfall depths (C; Table 2) and y_1, …, y_n be the corresponding forecasted rainfall depths from the product. If the product is probabilistic, the mean forecast for each pixel was calculated to allow a comparison with deterministic products.

That is, $y_i = \sum_{j=1}^{n_r} \frac{y_{i,j}}{n_r}$ where n_r is the number of probabilistic realizations (members) and $y_{i,j}$ is the simulated rainfall depth for j^{th} realization at the i^{th} pixel. The MSE was calculated as follows:

$$\mathrm{MSE} = \sum_{i=1}^{n} \frac{\left(y_i - x_i\right)^2}{n} = \sum_{i=1}^{n} \frac{\left(\left(y_i - x_i\right) - \left(\bar{y} - \bar{x}\right)\right)^2}{n} + \left(\bar{y} - \bar{x}\right)^2 \quad . \tag{3}$$

The two terms on the right-hand side of the equation correspond to the variance of the error (precision of the error) and the squared of the bias (accuracy), respectively.

For probabilistic products only, the Cumulative Rank Probability Score (CRPS; Matheson and Winkler, 1976) was calculated for each ensemble product and each group (Table 3) as follows:

$$\mathrm{CRPS} = \frac{1}{n} \sum_{i=1}^{n} \int_{t=-\infty}^{\infty} \left(F_i^{Y}(t) - F_i^{X}(t)\right)^2 \, dt \tag{4}$$

where $F_i^X(t)$ and $F_i^Y(t)$ are, for the i^{th} pixel of the group, the empirical cumulative distribution functions of the reference (C) rainfall depth (= 1 if $x_i \leq t$; = 0 otherwise) and of the ensemble forecasted rainfall depth, respectively. The CRPS allows for the evaluation of the mean accuracy of an ensemble product while also being sensitive to the width (precision of the probabilistic product) of the distribution (Hersbach, 2000).

Consistency of probabilistic products was evaluated via rank histograms (Talagrand diagrams). They are drawn for pixels with stratiform rainfall depth between 0.1 and 5 mm (Group 2, Table 3), for pixels with stratiform rainfall depth larger than 10 mm (Group 4) and for pixels with convective rainfall depth between 0.1 and 5 mm (Group 6). Rank histograms are not well suited for close-to-zero rainfall depths (Groups 1 and 5). Pixels with large convective rainfall depths (Group 7) were of interest, but there were not enough of them for rank histograms. Group 3 (pixels with stratiform rainfall depth between 5 and 10 mm) is not shown for sake of parsimony.

3 Results

3.1 Deterministic metric: MSE

As illustrated in Equation (3), MSE was broken down in order to verify the mean (bias; Figure 3) and the standard deviation of the error (Figure 4). The results regarding the CaPA-derived products illustrate that GSDM (Cd) reduced bias compared to the low-resolution product Ca, especially for large rainfall depths (Groups 4 and 7). The accuracy (Figure 3) and precision of the error (Figure 4) are also slightly higher for Cd compared to Cdn and even Cn, illustrating the ability of GSDM to generate rainfall depths close to the reference depth at fine scale. Note that all products underestimated the two pixel groups with the largest CaPA rainfall depths.

For RDPS forecasts, the bias of the product evaluated with respect to the neighborhood (Rn) was similar, although slightly higher, to that of the raw product (R) (Figure 3). The standard deviation of the error was lower for Rn than for R (Figure 4). In all likelihood, the lower standard deviations for Rn were due to the difference in the MSE calculation method; that is for the mean of the 121 ensemble members for Rn and for the unique deterministic value for R (Table 2). Thus, the standard deviation for Rn is smoothed, but the error of the product is not necessarily more precise. The bias of R was lower than that of the aggregated product (Ra), illustrating the added value of higher spatial-resolution forecasts. In all likelihood, the standard deviation of the error was smaller for Ra than for R, because the former values were spatially smoothed. Biases of the disaggregated RDPS products (Rd and Rdn) were similar to that of the raw product R.

Biases for the GEPS-derived forecasts were all very high (Figure 3). The coarse spatial resolution of the raw GEPS product (G) did not lead to smaller and larger intra-tile rainfall depths. The bias of G was larger than that of Ra, which has the same spatial resolution (about 100 km), but built using a forecast with higher spatial resolution (RDPS). Disaggregation (Gd and Gdn) did not provide a way to reduce the bias. As mentioned earlier, a suitable application of GSDM requires an accurate (unbiased), low-resolution, rainfall depth. Obviously, this assumption was not met for GEPS disaggregation.

3.2 Probabilistic metrics: CRPS and rank histograms

Ensembles produced by GSDM from aggregated CaPA analyses resulted in small CRPS values (Figure 5). Again, Cd slightly outperformed Cdn and even Cn; illustrating the ability of GSDM to produce accurate and precise ensemble rainfall depths at fine spatial scale. However, for stratiform events, Cdn outperformed Cd for consistency on pixels with rainfall depths between 0.1 and 5 mm (Figure 6) and larger than 10 mm (Figure 7). This latter figure shows that Cd too often underestimated pixels with large rainfall depths while Cdn did not have this issue. It suggests that GSDM may be not able to put the largest rainfall depths at the exact location, but it can generate these large rainfall depths in a neighboring area. For pixels with convective rainfall depths between 0.1 and 5 mm, consistency of Cd was better (Figure 8).

RDPS-derived forecasts had generally smaller CRPS values than those of GEPS-derived forecasts (Figure 5). For RDPS-derived forecasts, CRPS values were almost always smaller for Rd (RDPS disaggregated and evaluated at the target pixel) than for forecasts evaluated at the neighborhood pixels, disaggregated (Rdn) or not (Rn). However, Rd is not consistent for the three groups of pixels analyzed (Figures 6-8). For most of the pixels in each group, the reference value is either smaller than or equal to the first 5% or larger than the last 5% of the stochastic realizations. Rd overestimated too often pixels with stratiform rainfall depths between 0.1 and 5 mm (Figure 6). Rdn had better consistency than Rd, but just slightly lower than Rn (Figures 6-8). That being said, Rn overestimated pixels with convective rainfall depths between 0.1 and 5 mm (Figure 8). It suggests that RDPS produced too smooth forecasts for convective rainfall.

For GEPS-derived forecasts, CRPS values for Gd were also smaller than those for Gdn for stratiform rainfalls, but not for convective rainfalls. Consistency was weak for all GEPS-derived forecasts (Figures 6-8), except for Gdn for pixels with stratiform rainfall depths larger than 10 mm (Figure 7).

4 Discussion

The above results demonstrated the capacity of GSDM to generate accurate and precise ensemble rainfall depths at a local scale (10 km) for cases when spatially averaged reference rainfall (Ca) was used as input. The bias and the standard deviation of the error of the disaggregated product Cd always remained smaller than for the low-resolution reference product Ca used as input (Figures 3 and 4). Also, CRPS values for Cd were smaller than the reference ensemble Cn formed from 120 neighboring pixels (+/- 5 in each direction) (Figure 5). However, the disaggregated product Cd was not consistent for stratiform rainfall (Figures 6-7). Including the neighboring pixels in the disaggregated ensemble (Cdn) mitigated the lack of consistency, especially for large stratiform rainfall depths (Figure 7). For convective rainfall (Figure 8), Cd was consistent, thanks to the parameterization of GSDM which adjusts the spatial variability according to CAPE.

For the ECCC forecast products analyzed, despite a high bias for large convective rainfall depths (Figure 3), the regional 10-km resolution product (RDPS; R) outperformed the global 100-km resolution ensemble product (GDPS; G) based on accuracy and precision of the error criteria. However, RDPS is a deterministic product and does not provide uncertainty bands for end users. This issue was circumvented by building an ensemble with the RDPS rainfall depths forecasted in the neighboring area (Rn). Rn was relatively consistent for small stratiform rainfall depths (Figure 6), but not as much for large stratiform (Figure 7) and convective rainfall depths (Figure 8). Furthermore, GDPS ensemble was clearly not consistent (Figure 6-8).

While the added value of GSDM applied on low-resolution reference rainfall depths is clear, the added value of GSDM applied to ECCC forecasts was difficult to detect. GSDM did not reduce the bias of RDPS and GEPS forecasts (Figure 3). The Rd product, an ensemble at high-resolution (10 km) from the deterministic forecast RDPS, had smaller CRPS values than Rn, an ensemble formed by the raw RDPS rainfall depth in the neighboring pixels (Figure 5). However, consistency of Rd was not as strong compared to that of Rn (Figures 6-8). Including the neighboring pixels in the ensemble forecast (Rdn) increased the consistency. The added value of Rdn compared to Rn was the reduction of the bias for convective events (Figure 8). For GEPS, GSDM did not improve the forecast, except for the consistency of large stratiform rainfall depths, provided that the depths generated in the neighboring pixels be included in the ensemble (Gdn, Figure 7).

To summarize, none of the analyzed products provided entirely satisfactory outputs for short-term forecasts. That being said, there is potential for improvements. Integration of a Bayesian approach in GSDM parameter estimation and data assimilation represent one potential improvement. Instead of having the same parameter set for all realizations, the parameter values could be selected from a predefined random distribution for each realization. This would add some randomness to the disaggregated field, while keeping spatial coherence. Similarly, the assumption that the low-resolution rainfall depth used as input is reliable, which is realistic for reanalyses, but not necessarily true in a forecast mode, could be relaxed. Random perturbations could be generated at each realization for the mean areal rainfall depth used as input, as well as for wind speed, wind direction and CAPE values. Finally, neighboring pixels could still be considered, but the number of neighboring pixels could be reduced and/or vary depending on the type of event (stratiform or convective). However, in-depth analyses on the extent of the neighboring area were beyond the scope of this study.

From a wider perspective, ongoing improvements of meteorological modeling, including parameterization, data assimilation, spatial resolution, and uncertainty estimation, is at the heart of the matter. With better meteorological forecasts, new goals will become obtainable and spatial disaggregation models or other statistical downscaling techniques will remain of interest. Indeed, these techniques all need accurate input data. This work focused on derived products for end users by coupling GSDM with currently available meteorological products from ECCC. Meteorological model improvement was beyond the scope of this study.

5 Conclusion

A total of 30, 6-h, rainfall events within an area of about 40,000 km^2 were analyzed to evaluate accuracy, precision and consistency of the Gibbs Sampling Disaggregation Model (GSDM, Gagnon, 2012; Gagnon and Rousseau, 2014) coupled with Environment and Climate Change Canada (ECCC) meteorological short-term forecasts. The goal was to produce reliable information at local scale (10 km) for end users. GSDM ran sufficiently fast to provide an ensemble of rainfall fields for short-term forecasts.

Overall, GSDM applied with 100-km aggregated reference rainfall depths as input gave accurate (low bias) and precise (low variability of the error and low dispersion of the ensemble) 10-km fields. For small convective rainfall depths, GSDM was consistent (observed value indistinguishable of a randomly selected realization of the ensemble), but it could be improved for stratiform rainfall depths. When applied in forecast mode, GSDM inherited the bias of the meteorological forecast. In the end, the 10-km disaggregated rainfall depths from 100-km Global Ensemble Prediction System (GEPS) forecasts, which were found to be highly biased and imprecise, resulted in biased and imprecise information.

The Regional Deterministic Prediction System (RDPS) provided 10-km rainfall depths with moderate biases. It is worth noting that by aggregating RDPS forecasts to a 100-km spatial scale, biases evaluated on 10-km pixels slightly increased compared to the raw 10-km forecasts, but remained much smaller than those from 100-km GEPS forecasts. The

GSDM coupled with 100-km aggregated RDPS forecasts produced better results than with GEPS forecasts. However, despite this improvement, the disaggregated forecasts were not consistent. Including the 120 neighboring pixels in the disaggregated ensemble could help to mitigate the lack of consistency of the forecast, especially for convective rainfall.

Possible areas for improvements were identified, such as a Bayesian estimation of GSDM parameters, random perturbations of GSDM inputs and inclusion of a variable number of neighboring pixels in the ensemble, where the exact number could depend on the type of events. These improvements, once ascertained, would remain of interest even if meteorological models were improved.

The same analyses for different experimental set ups could produce different outcomes. In the present study, the area was mostly flat, except for the Appalachian Mountains in the south-east portion of the study region. Application in a more complex topographical region could require modifications to GSDM (Gagnon *et al.*, 2013). Also, if one is interested in 6-h rainfall depths at longer lead times (3, 10, 30 days), the meteorological forecast bias and imprecision should increase, resulting in a decrease in the reliability of the disaggregated rainfall depths. This effect could be reduced if one is interested in cumulative rainfall depths instead of a specific 6-h period. Longer time steps would smooth out the spatial variability and might increase the reliability of the forecasts, disaggregated or not.

Acknowledgements

This project was funded by the Discovery Grant program of the Natural Sciences and Engineering Research Council (NSERC) of Canada (Alain N. Rousseau, principal investigator). The authors would like to thank the anonymous reviewers and the associate editor for their helpful and constructive comments. The authors would also like to thank Alexandre Vanasse from Solutions Mesonet for providing calibration data.

References

Anderson, J.L. (1997). The impact of dynamical constraints on the selection of initial conditions on ensemble predictions: Low-order perfect model results. *Monthly Weather Review, 125*, 2969-2983.

Badas, M.G., R. Deidda, and E. Piga (2006). Modulation of homogeneous space-time rainfall cascades to account for orographic influences, *Natural Hazards and Earth System Sciences*, *6*, 427-437, ISSN: 1561-8633.

Baldauf, M., Seifert, A., Förstner, J., Majewski, D., and Raschendorfer, M. (2011). Operational convective-scale numeral weather prediction with the COSMO model: Description and sensitivities. *Monthly Weather Review*, *139*, 3887-3905.

Bauer, P., Thorpe, A., and Brunet, G. (2015). The quiet revolution of numerical weather prediction. *Nature*, *525*, 47-55.

Bendre, M.R., Thool, R.C., and Thool, V.R. (2015). Big data in precision agriculture: Weather forecasting for future farming. 2015 1st International Conference on Next

Generation Computing Technologies (NGCT), Dehradun, pp. 744-750. doi: 10.1109/NGCT.2015.7375220

Cai, J., Liu, Y., Lei, T., and Pereira, LS. (2007). Estimating reference evapotranspiration with the FAO Penman–Monteith equation using daily weather forecast messages. *Agricultural and Forest Meteorology*, *145*(1-2), 22-35.

Cai, X., Hejazi, M., and Wang, D. (2011). Value of Probabilistic Weather Forecasts: Assessment by Real-Time Optimization of Irrigation Scheduling. *Journal of Water Resources Planning and Management*, *137*(5), 391-403.

Caron, J.-F., Milewski, T., Buehner, M., Fillion, L., Reszka, M., Macpherson, S., and St-James, J. (2015). Implementation of Deterministic Weather Forecasting Systems based on Ensemble-Variational Data Assimilation at Environment Canada. Part II: The Regional System. *Monthly Weather Review*, *143*(7), 2560-2580.

Charron, M., Pellerin, G., Spacek, L., Houtekamer, P.L., Gagnon, N., Mitchell, H.L., and Michelin, L. (2010). Toward Random Sampling of Model Error in the Canadian Ensemble Prediction System. *Monthly Weather Review*, *138*, 1877-1901.

Charron, M., Parent, A., and Frenette, R. (2013). The Regional Ensemble Prediction System (REPS). RPN Seminar Series, Environment Canada, June 17^{th}, 2013.

Deidda, R. (2000). Rainfall downscaling in a space-time multifractal framework, *Water Resources Research*, *36*(7), 1779-1794, ISSN: 0043-1397.

Deidda, R., M.G. Badas, and E. Piga (2006a). Space-time Multifractality of Remotely Sensed Rainfall Fields, *Journal of Hydrology*, *322*, 2-13.

Deidda, R., Badas, M.G., Seoni, A., and Piga, E. (2006b). A meteo-hydrological forecasting chain: performance of the downscaling and rainfall-runoff steps in a small catchment. *Advances in Geosciences*, *7*, 361-369.

Fiorucci, P., La Barbera, P., Lanza, L.G., and Minciardi, R. (2001). A geostatistical approach to multisensor rain field reconstruction and downscaling. *Hydrology and Earth System Sciences*, *5*(2), 201-213.

Forman, B.A., Vivoni, E.R., and Margulis, S.A. (2008). Evaluation of ensemble-based distributed hydrologic model response with disaggregated precipitation products. Water Resources Research, *44*, W12409.

Fortin, V., G. Roy, N. Donaldson and A. Mahidjiba (2015). Assimilation of radar quantitative precipitation estimations in the Canadian Precipitation Analysis (CaPA). *Journal of Hydrology*, *531*(2), 296–307.

Gaborit, E., Anctil, F., Fortin, V., and Pelletier, G. (2014). Hydrologic evaluation of spatially disaggregated global ensemble rainfall forecasts. *Hydrological Processes*, *28*(17), 4682-4693.

Gagnon, P. (2012). Désagrégation statistique de la précipitation mésoéchelle. Ph. D. thesis. Institut National de la Recherche Scientifique, Centre eau, terre et environnement, Université du Québec, Québec city, PQ, Canada, 245 pp. [in French]

Gagnon, P., Rousseau, A.N., Mailhot, A., and Caya, D. (2012). Spatial disaggregation of mean areal rainfall using Gibbs sampling. *Journal of Hydrometeorology*, *13*(1), 324-337.

Gagnon, P., Rousseau, A.N., Mailhot, A., and Caya, D. (2013). A Gibbs sampling disaggregation model for orographic precipitation. *Journal of Applied Earth Observation and Geoinformation*, *22*(1), 16-26.

Gagnon, P., and Rousseau, A.N. (2014). Stochastic spatial disaggregation of extreme precipitation to validate a Regional Climate Model and to evaluate climate change impacts over a small watershed. *Hydrology and Earth System Sciences*, *18*, 1695-1704.

Geman, S., and Geman, D. (1984). Stochastic relaxation, Gibbs distribution and the Bayesian restoration of images. *IEEE Transactions on Pattern Analysis Machine and Intelligence*, *6*(6), 721-741.

Groppelli, B., Bocchiola, D., and Rosso, R. (2011). Spatial downscaling of precipitation from GCMs for climate change projections using random cascades: A case study in Italy. *Water Resources Research*, *47*, W03519.

Gupta, V. K., and E. C. Waymire (1993), A statistical analysis of mesoscale rainfall as a random cascade, *Journal of Applied Meteorology*, *32*, 251-267.

Harris, D., and Foufoula-Georgiou, E. (2001). Subgrid variability and stochastic downscaling of modeled clouds: Effects on radiative transfer computations for rainfall retrieval, *Journal of Geophysical Research*, *106*(D10), 10349-10362.

Hersbach, H. (2000). Decomposition of the Continuous Ranked Probability Score for Ensemble Prediction Systems. *Weather Forecasting*, *15*, 559-570.

Houtekamer, P.L., Deng, X., Mitchell, H.L., Baek, S.J., and Gagnon, N. (2014). Higher Resolution in an Operational Ensemble Kalman Filter, *Monthly Weather Review*, *142*, 1143-1162.

Hubert, P., Tessier, Y., Lovejoy, S., Schertzer, D., Schmitt, F., Ladoy, P., Carbonnel, J.P., Violette, S., and Desurosne, I. (1993). Multifractals and extreme rainfall events, *Geophysical Research Letters*, *20*(10), 931-934.

Lovejoy, S., and Schertzer, D. (2010a). On the simulation of continuous in scale universal multifractals, part I: Spatially continuous processes. *Computers and Geosciences*, *36*(11), 1393-1403.

Lovejoy, S., and Schertzer, D. (2010b). On the simulation of continuous in scale universal multifractals, part II: Space-time processes and finite size corrections. *Computers and Geosciences*, *36*(11), 1404-1413.

Kumar, P., and Foufoula-Georgiou, E. (1993a). A multicomponent decomposition of spatial rainfall fields, 1, Segregation of large- and small- scale features using wavelet tranform, *Water Resources Research*, *29*(8), 2515-2532.

Kumar, P., and Foufoula-Georgiou, E. (1993b). A multicomponent decomposition of spatial rainfall fields, 2, Self-similarity in fluctuations, *Water Resources Research*, *29*(8), 2533-2544.

Mailhot, J., Bélair, S., Charron, M., Doyle, C., Joe, P., Abrahamowicz, M., Bernier, N.B., Denis, B., Erfani, A., Frenette, R., Giguère, A., Isaac, G.A., McLennan, N., McTaggart-Cowan, R., Milbrandt, J., and Tong, L. (2010). Environment Canada's Experimental

Numerical Weather Prediction Systems for the Vancouver 2010 Winter Olympic and Paralympic Games. *Bulletin of the American Meteorological Society*, *91*, 1073-1085.

Marsan, D., Schertzer, D., and Lovejoy, S. (1996). Casual space-time multi-fractal processes: Predictability and forecasting of rain fields, *Journal of Geophysical Research*, *101*(D21), 26,333-26,346.

Matheson, J.E., and Winkler, R.L. (1976). Scoring rules for continuous probability distributions. *Management Science*, *22*, 1087-1095.

Niemi, T.J., Guillaume, J.H.A., Kokkonen, T., Hoang, T.M.T., and Seed, A.W. (2016). Role of spatial anisotropy in design storm generation: Experiment and interpretation, *Water Resources Research*, *52*, 69-89.

Olson, J., and Niemczynowicz, J. (1996). Multifractal analysis of daily spatial rainfall distributions, *Journal of Hydrology*, *187*, 29-43.

Over, T.M., and Gupta, V.K. (1996). A space-time theory of mesoscale rainfall using random cascades. *Journal of Geophysical Research*, *101*(D21), 26319-26331.

Paschalis, A., Molnar, P., Fatichi, S., and Burlando, P. (2013). A stochastic model for high-resolution space-time precipitation simulation. *Water Resources Research*, *49*, 8400-8417.

Peleg, N., and Morin, E. (2014). Stochastic convective rain-field simulation using a high-resolution synoptically conditioned weather generator (HiReS-WG). *Water Resources Research*, *50*(3), 2124-2139.

Perica, S., and Foufoula-Georgiou, E. (1996). Model for multiscale disaggregation of spatial rainfall based on coupling meteorological and scaling descriptions. *Journal of Geophysical Research*, *101*(D21), 26347-26361.

Roberts, G.O. and Smith, A.F.M. (1994). Simple conditions for the convergence of the Gibbs sampler and Metropolis-Hastings algorithms, *Stochastic Processes and Their Applications*, *49*, 207-216.

Silva, D., Meza, F.J., and Varas, E. (2010). Estimating reference evapotranspiration (ETo) using numerical weather forecast data in Central Chile. *Journal of Hydrology*, *382*, 64-71.

Tables

Table 1. Main characteristics of the 30 GEPS events analyzed. The values are the averages from the four 100-km grid cells analyzed (2 x 2 central grid cells in Figure 2).

Date/Time (UTC)	Rainfall depth (mm/6h)	CAPE (J/kg)	Wind at 700 hPa Speed (m/s)	Wind at 700 hPa Direction (°)	Date/Time (UTC)	Rainfall depth (mm/6h)	CAPE (J/kg)	Wind at 700 hPa Speed (m/s)	Wind at 700 hPa Direction (°)
2015-07-18 6:00	3.2	1	13.0	223	2015-09-14 6:00	3.2	16	5.9	198
2015-07-18 12:00	5.6	108	14.3	260	2015-09-14 12:00	6.1	5	7.9	100
2015-07-20 0:00	4.7	1475	13.8	273	2015-09-20 6:00	4.6	32	21.7	236
2015-07-26 6:00	4.9	45	12.4	270	2015-09-20 12:00	4.9	0	15.6	253
2015-07-26 12:00	10.0	79	10.3	248	2015-09-30 0:00	9.5	44	13.6	233
2015-07-30 18:00	7.1	593	13.8	238	2015-09-30 6:00	8.1	9	11.2	253
2015-08-04 0:00	4.1	392	15.0	224	2015-09-30 12:00	20.6	0	6.2	238
2015-09-03 12:00	4.2	568	8.4	293	2015-09-30 18:00	11.0	0	4.4	211
2015-09-09 0:00	3.6	305	10.5	239	2015-10-01 0:00	12.8	0	7.8	175
2015-09-10 0:00	4.6	161	13.6	254	2015-10-17 12:00	3.4	0	12.7	238
2015-09-11 12:00	4.1	2	4.9	240	2015-10-25 12:00	6.2	0	23.4	229
2015-09-13 0:00	3.8	56	9.8	223	2015-10-29 0:00	8.2	0	28.9	226
2015-09-13 6:00	8.9	24	10.0	193	2015-10-29 6:00	8.9	0	28.3	219
2015-09-13 12:00	11.4	7	8.3	192	2015-10-29 12:00	14.2	75	21.5	223
2015-09-14 0:00	3.3	154	9.2	197	2015-11-14 0:00	3.22	0	15.1	280

Table 2. Description of the rainfall series analyzed. Raw ECCC products appear in boldface. For rainfall products aggregated before disaggregation (Cd, Cdn, Rd, Rdn), wind and CAPE data were aggregated as well.

ID	Source	Resolution	Nr of members of the ensemble
C	**CaPA**	**10 km**	**1 (deterministic, reference)**
Cn	CaPA	10 km	120 neighboring pixels
Ca	CaPA aggregated	100 km	1 (deterministic)
Cd	CaPA aggregated/disaggregated	10 km	100 random realizations
Cdn	CaPA aggregated/disaggregated	10 km	12,100 = 100 random realizations x 121 neighboring pixels
R	**RDPS**	**10 km**	**1 (deterministic)**
Rn	RDPS	10 km	121 neighboring pixels
Ra	RDPS aggregated	100 km	1 (deterministic)
Rd	RDPS aggregated/disaggregated	10 km	100 random realizations
Rdn	RDPS aggregated/disaggregated	10 km	12,100 = 121 neighboring pixels x 100 random realizations
G	**GEPS**	**100 km**	**21 members**
Gd	GEPS disaggregated	10 km	105 = 21 members x 5 realizations
Gdn	GEPS disaggregated	10 km	12,705 = 121 neighboring pixels x 21 members x 5 realizations

Table 3. Groups of pixels on which performance metrics were calculated.

Type of events	Group ID	CaPA rainfall depth (mm)	Number of pixels
Stratiform (CAPE < 500 J/kg)	1	[0, 0.1)	2180
	2	[0.1, 5)	4635
	3	[5, 10)	2000
	4	> 10	1885
		Total stratiform	10,700 (111 tiles)
Convective (CAPE > 500 J/kg)	5	[0, 0.1)	742
	6	[0.1, 5)	409
	7	> 5	149
		Total convective	1,300 (13 tiles)
		Total	12,000 (120 tiles = 30 events x 4 tiles/event)

Figure Captions

Figure 1. Example of a 6-h rainfall event: depths from the 10-km reference data (left panel), the aggregated 100-km reference data used as input by GSDM (middle panel) and a realization of GSDM at 10-km (right panel).

Figure 2. Study area with the 40 x 40 10-km pixels (dotted lines) in the 4 x 4 100-km grid cells (solid lines). The Bécancour watershed is shown for illustrative purposes.

Figure 3. Absolute value of the mean error (bias) (i.e. rainfall depth difference with the reference depth C) of all products for the seven groups of pixels. IDs of the rainfall products are defined in Table 2. IDs of the seven groups of pixels are defined in Table 3.

Figure 4. Standard deviation of the error of all products for the seven groups of pixels. IDs of the rainfall products are defined in Table 2. IDs of the seven groups of pixels are defined in Table 3.

Figure 5. Mean CRPS values of the ensemble products for the seven groups of pixels. IDs of the rainfall products are defined in Table 2. IDs of the seven groups of pixels are defined in Table 3.

Figure 6. Rank histograms of each ensemble product for group of pixels 2 (stratiform rainfall depth between 0.1 and 5 mm; 4635 pixels). The dashed line illustrates a rank histogram for a perfectly consistent ensemble product.

Figure 7. Rank histograms of each ensemble product for group of pixels 4 (stratiform rainfall larger than 10 mm; 1885 pixels). The dashed line illustrates a rank histogram for a perfectly consistent ensemble product.

Figure 8 Rank histograms of each ensemble product for group of pixels 6 (convective rainfall depth between 0.1 and 5 mm; 409 pixels). The dashed line illustrates a rank histogram for a perfectly consistent ensemble product.

Figure 1

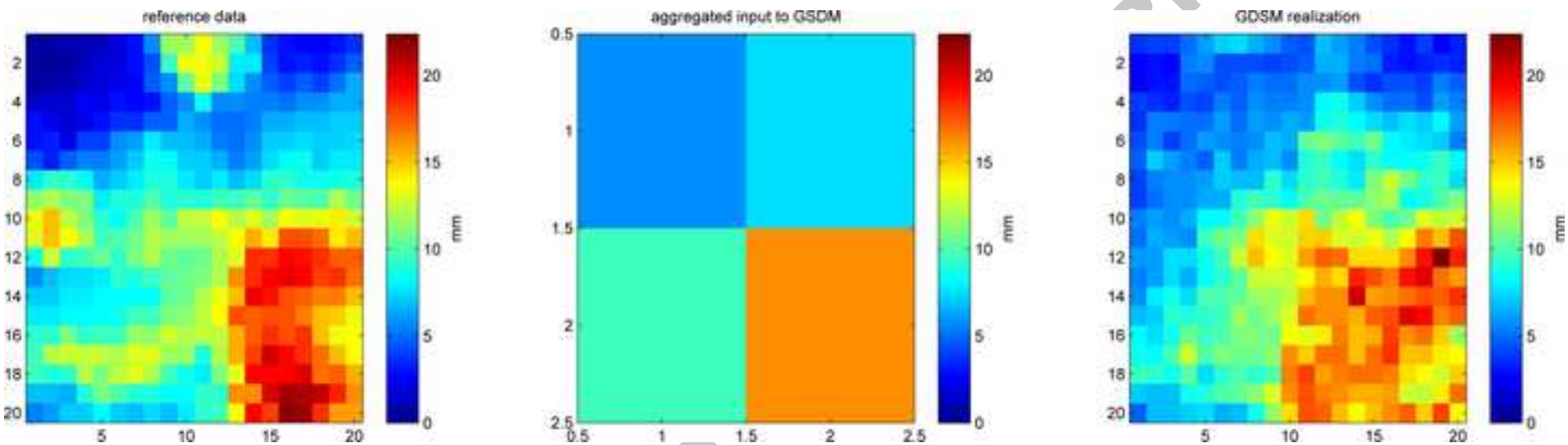
reference data
aggregated input to GSDM
GDSM realization
mm
0
5
10
15
20
0.5
1
1.5
2
2.5

Figure 2

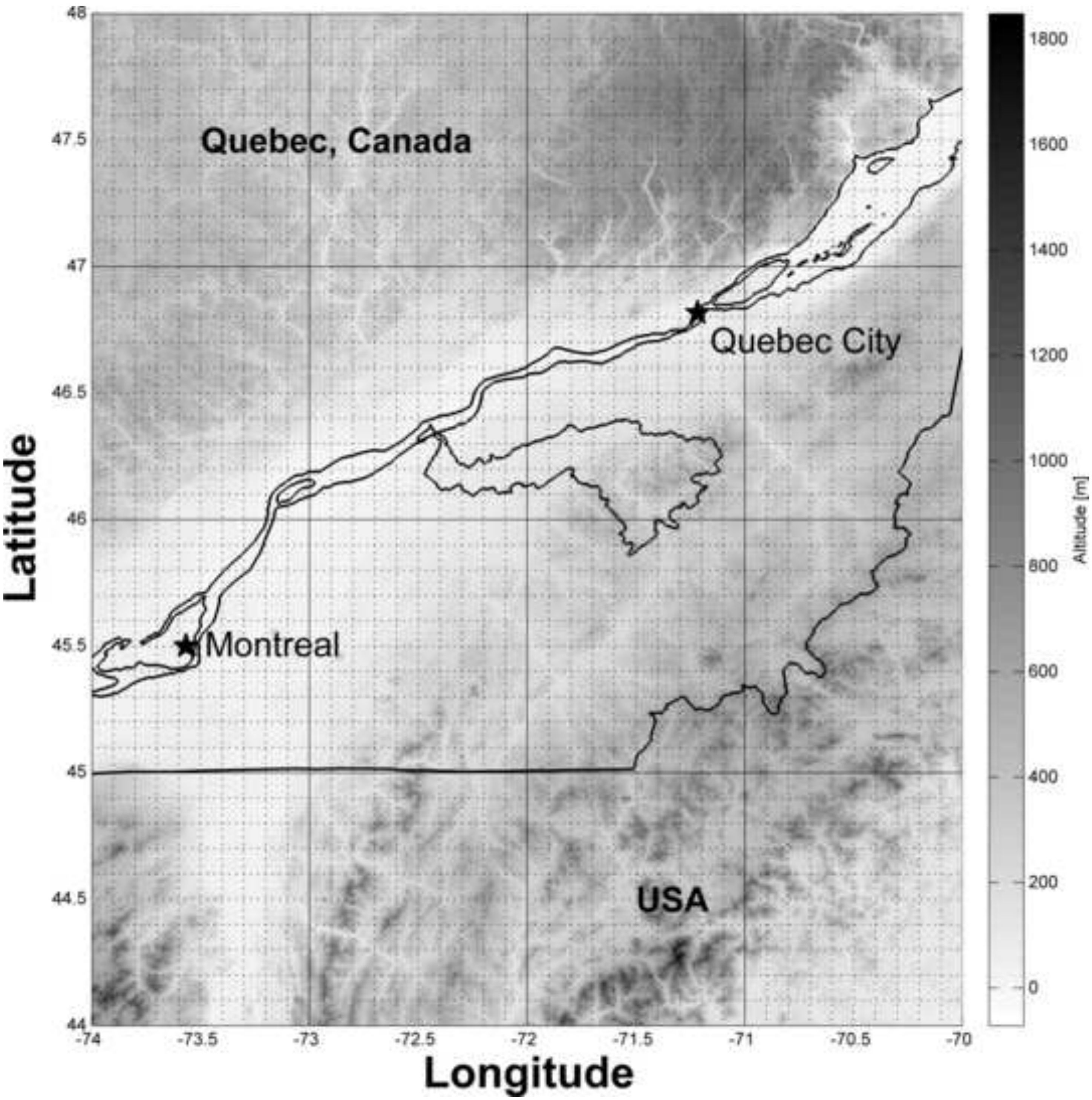

Quebec, Canada
Quebec City
Montreal
USA
Latitude
Longitude
Altitude [m]
48
47.5
47
46.5
46
45.5
45
44.5
44
-74
-73.5
-73
-72.5
-72
-71.5
-71
-70.5
-70
1800
1600
1400
1200
1000
800
600
400
200
0

Figure 3

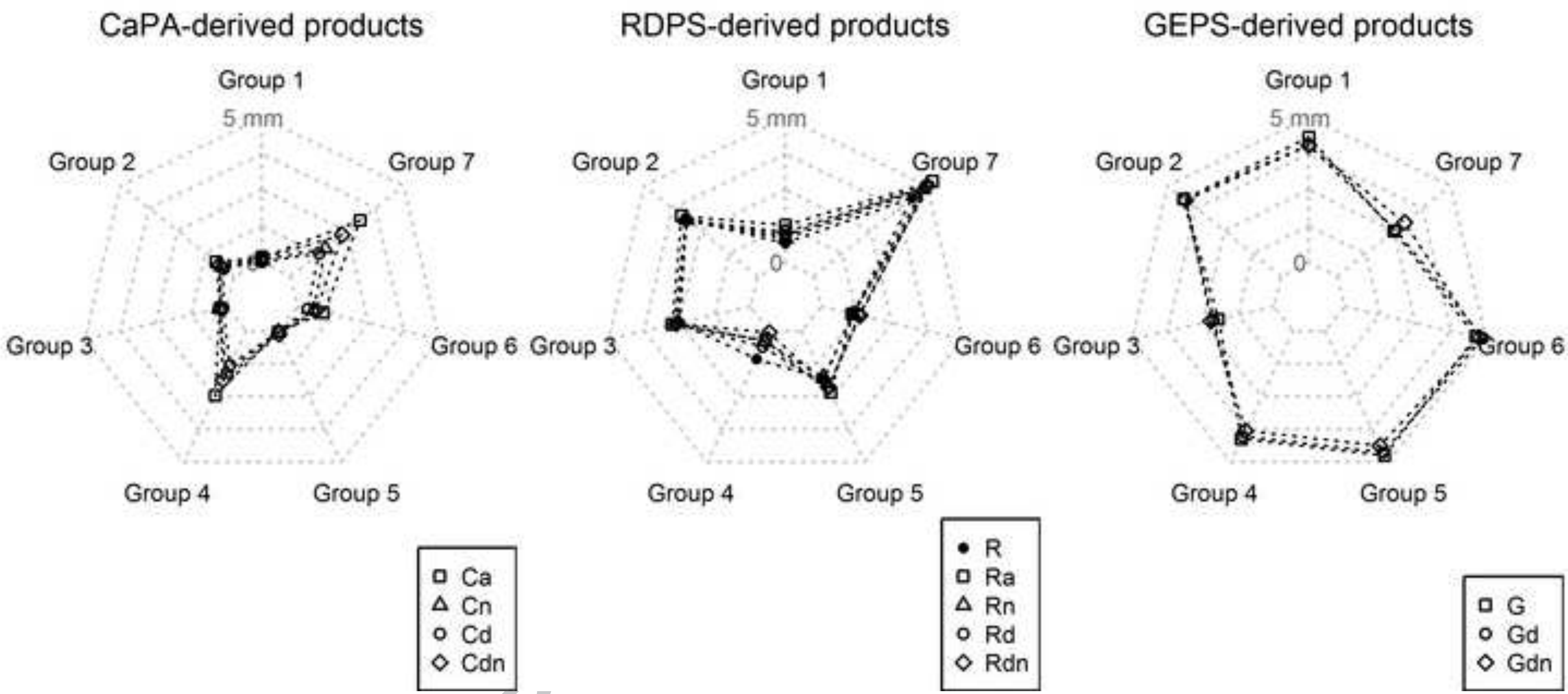
CaPA-derived products
RDPS-derived products
GEPS-derived products
Group 1
Group 2
Group 3
Group 4
Group 5
Group 6
Group 7
5 mm
0
Ca
Cn
Cd
Cdn
R
Ra
Rn
Rd
Rdn
G
Gd
Gdn

Figure 4

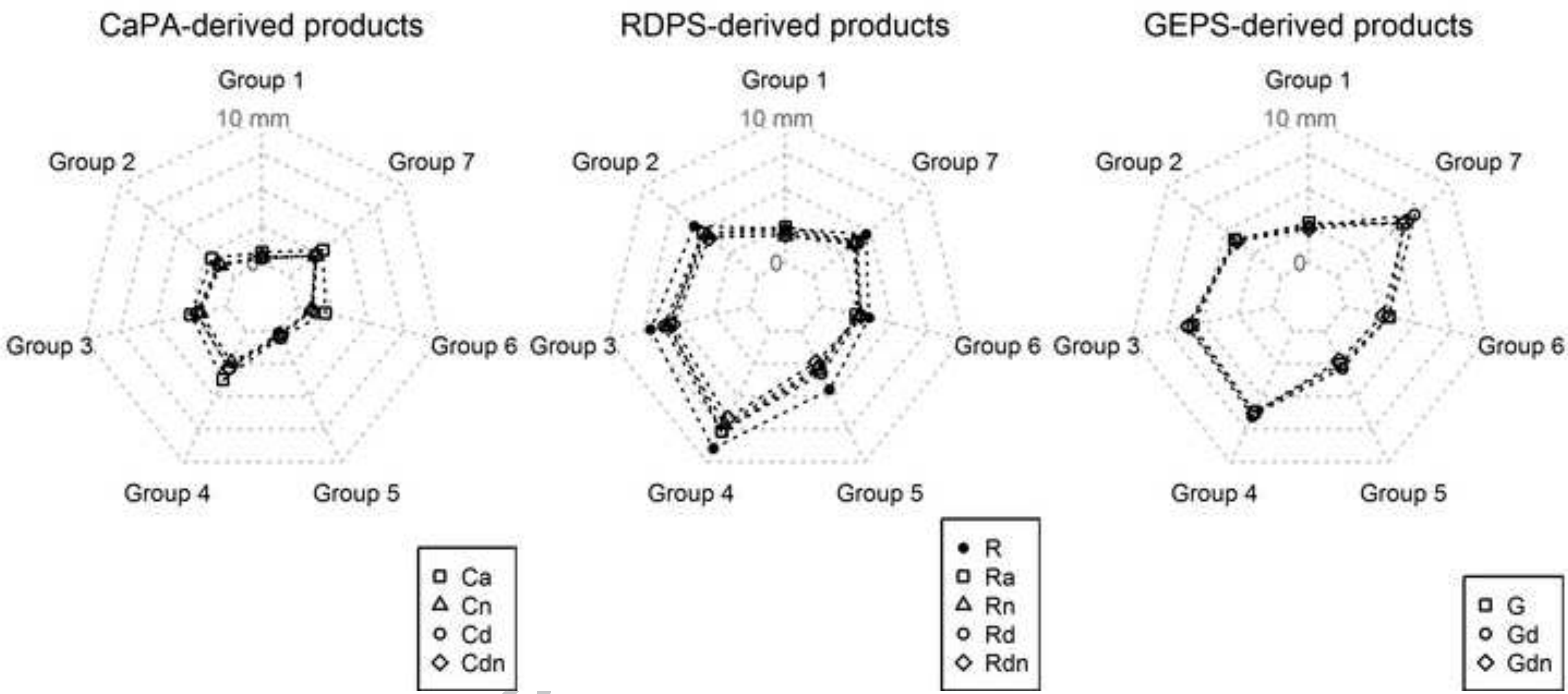
CaPA-derived products
Group 1
10 mm
Group 2
Group 7
0
Group 3
Group 6
Group 4
Group 5
Ca
Cn
Cd
Cdn
RDPS-derived products
Group 1
10 mm
Group 2
Group 7
0
Group 3
Group 6
Group 4
Group 5
R
Ra
Rn
Rd
Rdn
GEPS-derived products
Group 1
10 mm
Group 2
Group 7
0
Group 3
Group 6
Group 4
Group 5
G
Gd
Gdn

Figure 5

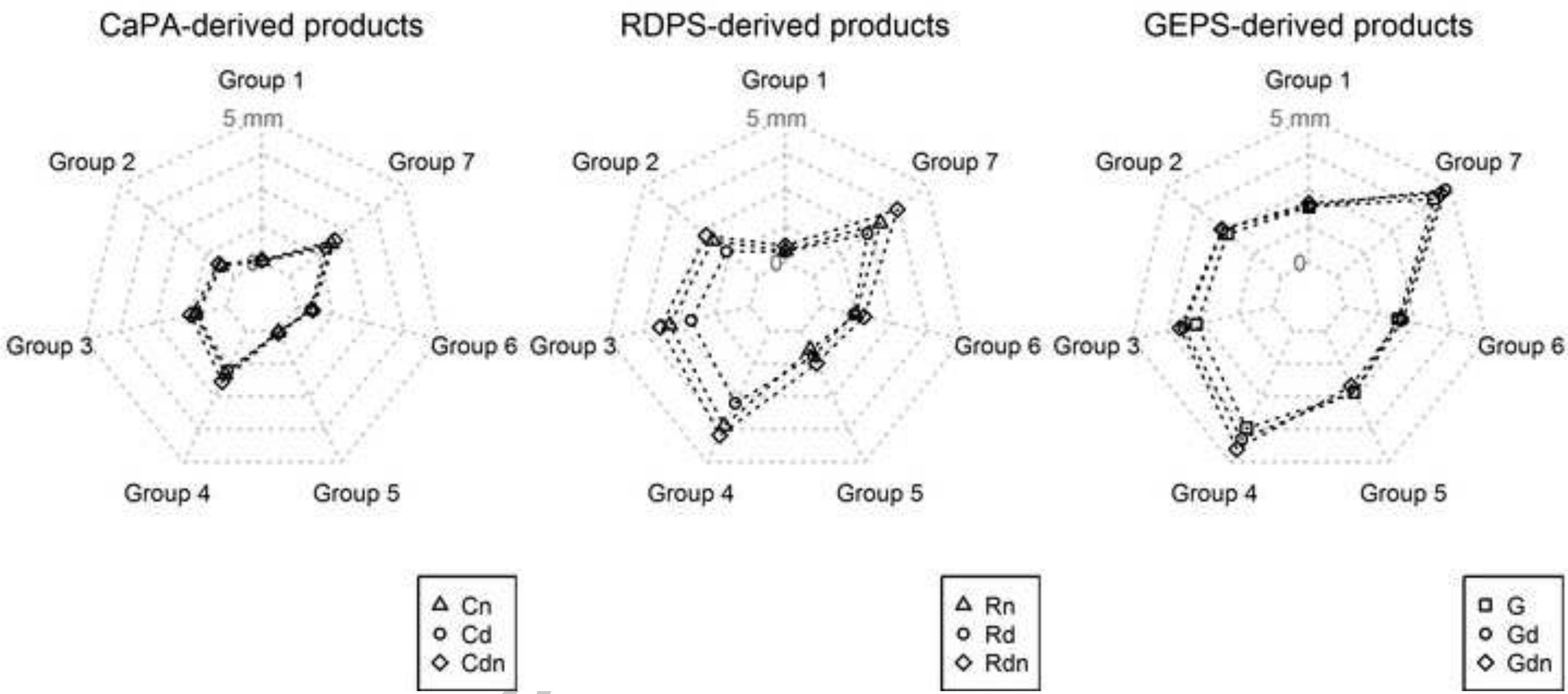
CaPA-derived products
RDPS-derived products
GEPS-derived products
Group 1
5 mm
0
Group 2
Group 3
Group 4
Group 5
Group 6
Group 7
Cn
Cd
Cdn
Rn
Rd
Rdn
G
Gd
Gdn

Figure 6

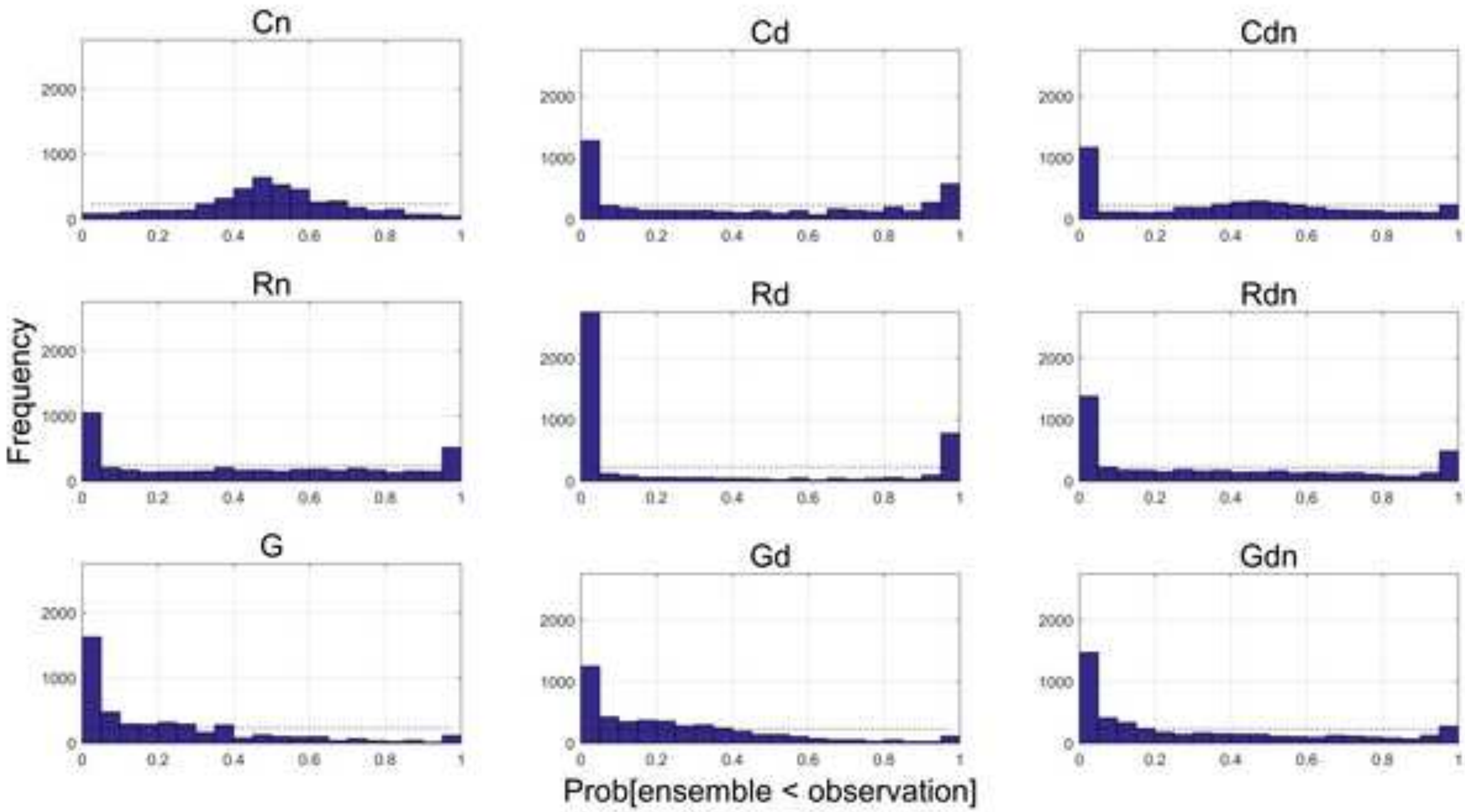
Cn
Cd
Cdn
Rn
Rd
Rdn
G
Gd
Gdn
Frequency
Prob[ensemble < observation]
0
1000
2000
0
0.2
0.4
0.6
0.8
1

Figure 7

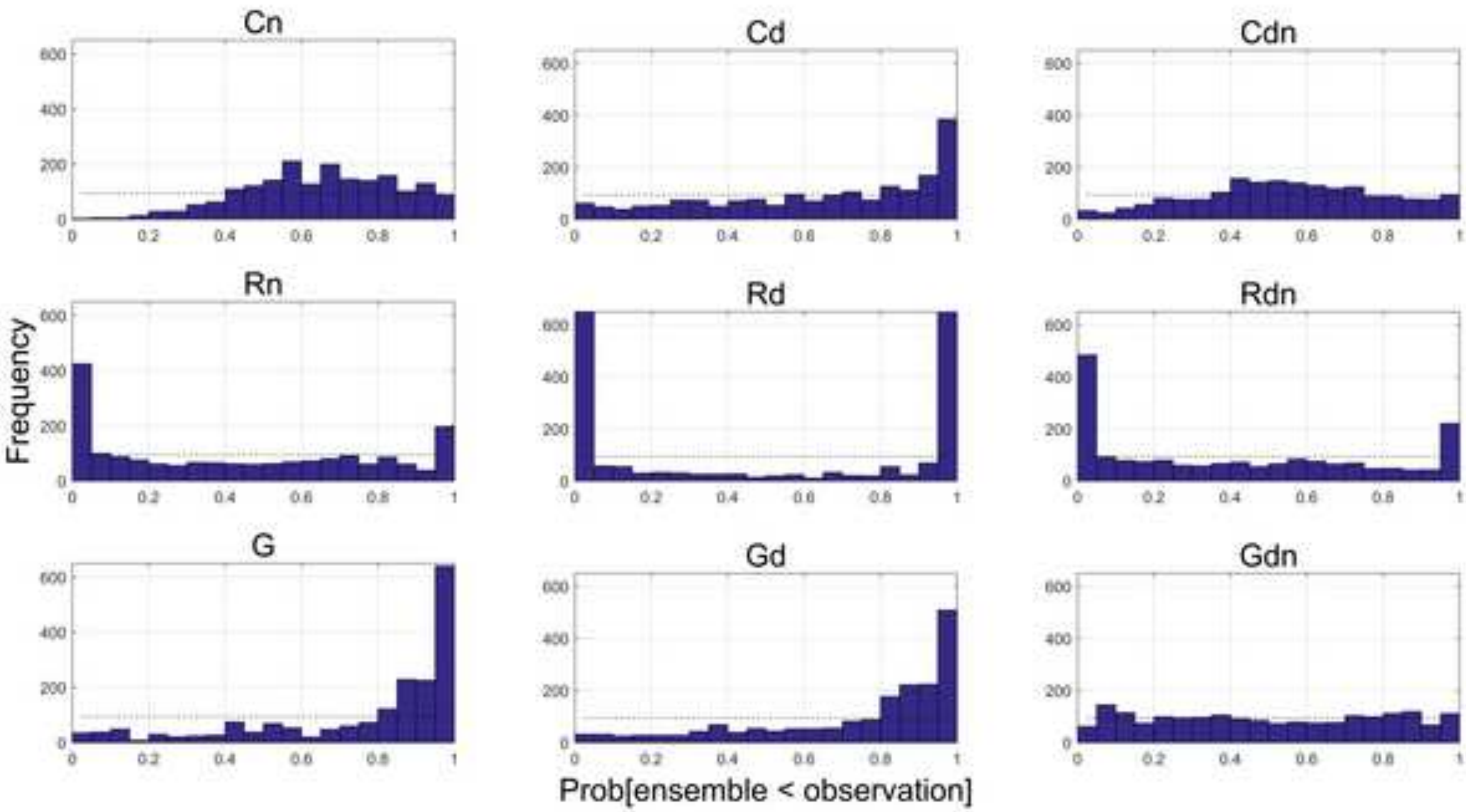
Cn
Cd
Cdn
Rn
Rd
Rdn
G
Gd
Gdn
Frequency
Prob[ensemble < observation]
0
200
400
600
0.2
0.4
0.6
0.8
1

Figure 8

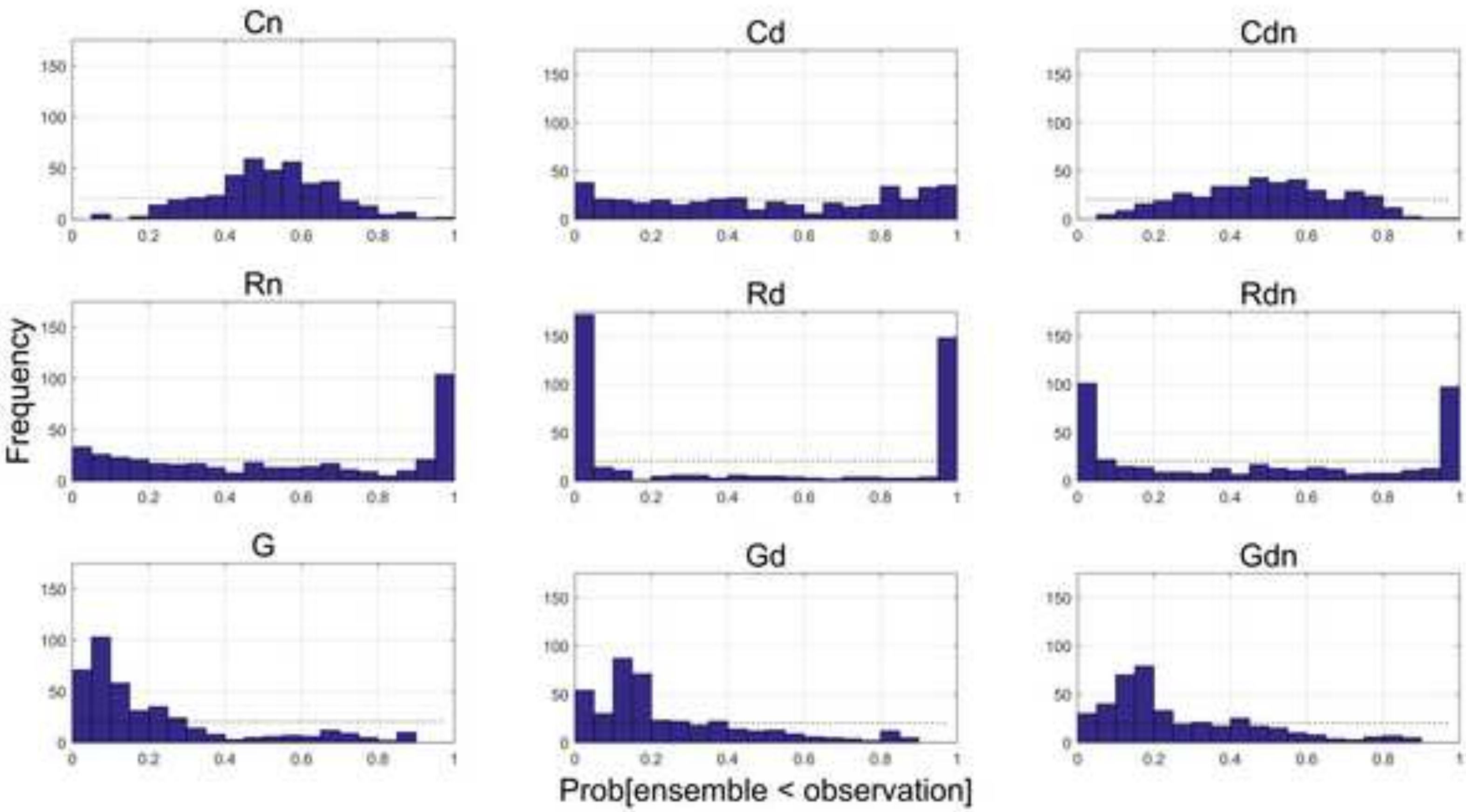
Cn
Cd
Cdn
Rn
Rd
Rdn
G
Gd
Gdn
Frequency
Prob[ensemble < observation]
150
100
50
0
0
0.2
0.4
0.6
0.8
1

Highlights

- GSDM applied on reference data generates accurate and precise rainfall fields
- GSDM inherits of the forecast bias
- Global ensemble forecasts (GEPS) are not consistent, with or without GSDM
- GSDM performance was better with regional deterministic forecasts (RDPS)
- Neighboring pixels should be considered when producing high-resolution ensembles